Iraqi National Journal of Earth Science

www.earth.mosuljournals.com

Seismic Refraction Tomography and Geotechnical Parameters to Assess the Chaqchaq Dam failure in NW Sulaimani City, Kurdistan Region, Iraq

Ezzadin N. Baban [1], Abdulla K. Amin [2], Sazan S. Mohammed [3]

[1,3] *Department of Geology, College of Science, University of Sulaimani, Sulaimani, Iraq.*

[2] *Department of social sciences, College of basic education, University of Sulaimani, Sulaimani, Iraq.*

Article information

Received: 16- Aug -2022

Accepted: 23- Oct -2022

Available online: 31- Dec- 2022

Keywords:
Seismic refraction tomography
Primary wave velocity
Chaqchaq dam
Sulaimani
Iraqi Kurdistan Region

Correspondence:
Name: Ezzadin N. Baban
ezadin.mohamed@univsul.edu.iq

ABSTRACT

This study is conducted along fifteen seismic refraction traverses in the reservoir part of the failed Chaqchaq dam NW of Sulaimani City. The results show that the area consists of three geological layers. The first layer consists of soil with a thickness ranging between 0.05-3.10m, whereas the second layer consists of rock fragments ranging between 1.93-13.11m and the third layer is specified as a consolidated and cohesive limestone of the Kometan Formation that lies at a depth ranging between 2.0-16.2m. The Kometan limestone surface is irregular due to weathering and fracture as a result of tectonic movement leading to the collapse of the area and later on filled with sediments of recent deposits, or maybe decamped by water then karstification occurred.

Based on the estimated geotechnical parameters from Vp and Vs and measured density, the result will indicate that the first and second layers is weak and fissured and subjected to sinkholes buried with recent sediments. Whereas the third layer indicates the harder-to-fracture rocks, the research would find the linear relationship between Vp and Vs of the first, second, and third layers. The relationships between Poisson's ratio and Vs/Vp for the first layer and Vs/Vp for the second layer are pointed as inverse relationships. This means that increasing Poisson's ratios reduces both Vs/Vp ratio and the brittleness of the materials. Also, the elastic modulus and shear (rigidity) modulus as well as bulk modulus values are directly proportional with increasing depth, especially within the hard and cohesive Kometan Fn.

The results also show the basic design of the dam construction was not done scientifically. The beginning parts of most traverses appear to the presence of sinkhole that was related to the filling of the layers with water during the winter rainy season and then penetrating deeply, which leads to the collapse of the layer and forming this sinkhole, this sinkhole can be considered as the reason for the dam collapsing.

DOI: 10.33899/earth.2022.135251.1027,

استخدام التصوير المقطعي الانكساري الزلزالي والمعاملات الجيوتقنية لتقييم فشل سد جقجق في شمال غرب مدينة السليمانية، إقليم كردستان العراق

عزالدين نجم الدين بابان[1]، عبدالله كريم امين[2]، سازان صفاء محمد[3]

[1، 3] قسم علوم الأرض، كلية العلوم، جامعة السليمانية، السليمانية، العراق

[2] قسم العلوم الاجتماعية، كلية التربية الأساسية، جامعة السليمانية، السليمانية، العراق

معلومات الارشفة

تاريخ الاستلام: 16- أغسطس-2022

تاريخ القبول: 23- أكتوبر-2022

تاريخ النشر الالكتروني: 31- ديسمبر-2022

الكلمات المفتاحية:

الزلزالية الانكسارية التصويرية

سرعة الموجات الطولية والعرضية

سد جقجق

السليمانية

اقليم كردستان العراق

المراسلة:

الاسم: عزالدين نجم الدين بابان

ezadin.mohamed@univsul.edu.iq

الملخص

أجريت هذه الدراسة على امتداد خمسة عشر مسار انكسار زلزالى فى الجزء المكمن لسد جقجق المنهار شمال غرب مدينة السليمانية. أظهرت النتائج أن المنطقة تتكون من ثلاث طبقات جيولوجية. تتكون الطبقة الأولى من تربة بسمك يتراوح بين 0.05-3.10 م، بينما تتكون الطبقة الثانية من شظايا صخرية تتراوح ما بين 1.93-13.11 م والطبقة الثالثة محددة على أنها حجر جيرى متماسك من تكوين كوميتان يقع على عمق يتراوح بين 2.0-16.2 م. سطح الحجر الجيرى لكوميتان غير منتظم نتيجة لحدوث الحركات التكتونية التي حدثت في المنطقة ومن ثم تعرضها لعوامل التجوية والتعرية، وامتلئت برواسب الرواسب الحديثة، أو ربما تكونت ظواهر كظواهر كارست Karst وحفر مدفونة sinkholes. بناءً على المعلمات الجيوتقنية المقدرة من Vp وVs والكثافة المقاسة، ستشير النتيجة إلى أن الطبقة الأولى ضعيفة ومتشققه ومعرضة لحفر وكهوف مدفونة مع الرواسب الحديثة. بينما تشير الطبقة الثالثة إلى صعوبة تكسير الصخور، تم ايجاد العلاقة الخطية بين Vp وV للطبقات الأولى والثانية والثالثة. يشار إلى العلاقات بين نسبة Poisson وVs / Vp للطبقة الأولى وVs / Vp للطبقة الثانية هي علاقات عكسية. هذا يعنى أن زيادة نسب بواسون تقلل من نسبة Vs / Vp وهشاشة المواد، كما أن معامل المرونة ومعامل القص (الصلابة) فضلا عن قيم معامل التغير الحجمي كانت متناسبة بشكل مباشر مع العمق خاصةً داخل تكوين كوميتان الصلب. كما أظهرت النتائج أن التصميم الأساسى لبناء السد لم يتم بطريقة علمية. تظهر الأجزاء الأولى من المسارات اظهرت حفرامتلئت بالمياه خلال موسم الأمطار الشتوى ثم توغلت بعمق مما أدى إلى انهيار الطبقة وتشكيل هذا المجرى الذى كان يعتبر أحد أسباب الانهيار.

DOI: 10.33899/earth.2022.135251.1027,

Introduction

The study area (upstream) of the failed Chaqchaq Dam is located about 2 km NW of Sulaimani City of the Kurdistan Region, NE Iraq. Geographically, it lies in the degree coordinates system between latitudes 3939971 m N - 3940267 m N and longitudes 38S 534650 m E - 38S 534830 m E, which covers an area of about 45,039 m^2 having an elevation ranging between 768 to 773 m as in (Fig. 1). The dam built in the valley of Chaqchaq stream that falls between plunge of Sulaimani anticline. This anticline lies on the western and eastern sides of the dam due to a strike-slip fault that cuts the Sulaimani Anticline (Al-Hakari, 2011). The topography of the study area is approximately flat having small undulation and sloping from the eastern to the western side of the upstream dam.

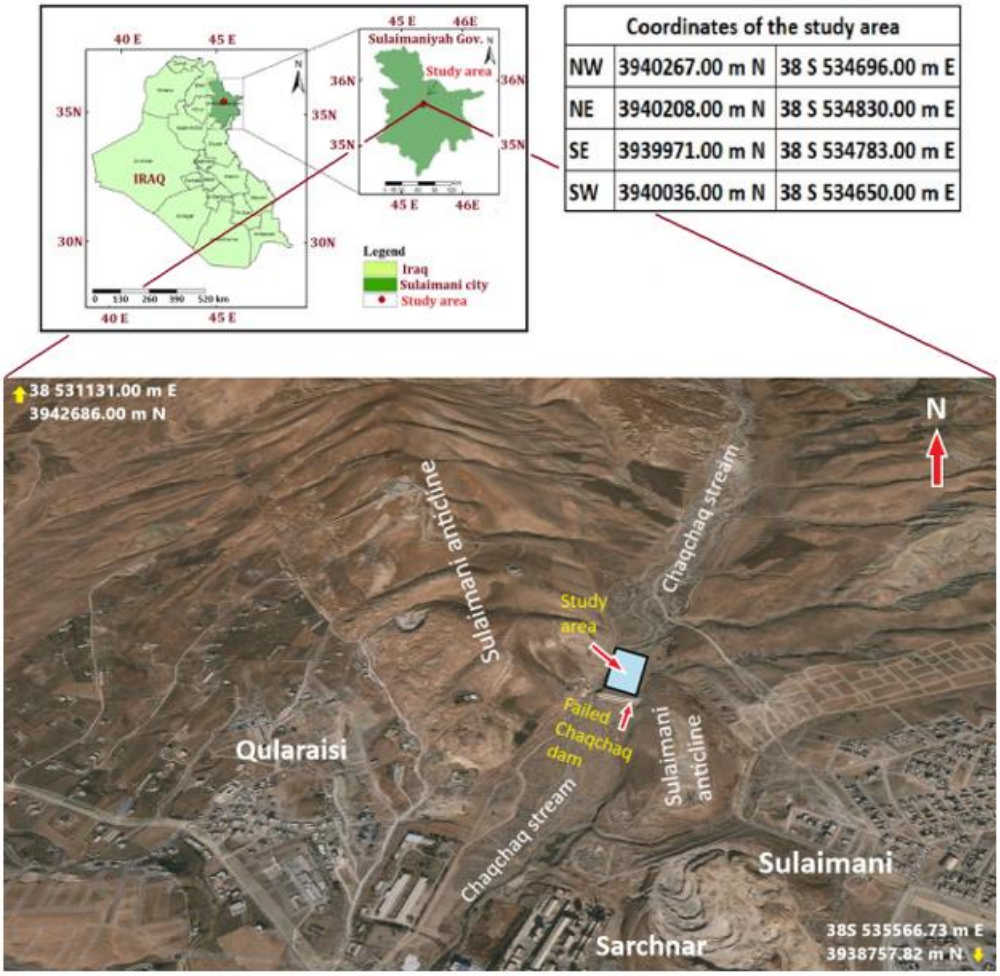

Fig. 1. Location map of the study area (Google earth, 2022).

The collapsed Chaqchaq dam is one of those core clay body small dams constructed by the KRG on the Qiliasan stream, 2 km NW of Sulaimani City. This dam was more beneficial for flood control, irrigation, tourism, and drinking water. Abdulrahman (2014) reported on 4th February 2006 at about 10:00 P.M. this dam failed due to overtopping. Abdelwahed (2019) pointed out that design and construction are fundamental to preventing the collapse of the structure. According to James, et al. (1986), dams may fail or suffer significant damage due to floods and earthquakes.

Physical features in the subsurface fluctuate in response to lithological, structural, and mechanical changes, which can be identified using geophysical techniques. Sarris, et al. (2018) considered geophysical explorations are a means of collecting broad subsurface geology information that is obtained indirectly. Since the 1920s, geophysical methods had been employed in dam site surveys and safety monitoring. Adamo, et al. (2020) regarded good alternatives to standard geotechnical methods for performing observation duties on existing dams in a non-intrusive, considerably quicker, and less expensive manner. Many researchers used the seismic refraction tomography (SRT) method to delineate subsurface features through the earth dam. Brosten et. al. (2005) reported that seismic refraction surveying is used to map the subsurface from recorded data using mechanical vibrations. Sharafeldin (2008) applied a 2D-seismic refraction survey to study the bedrock conditions of a proposed dam and reservoir site in Wadi Asala, Jeddah area, Saudi Arabia. Uyank (2011) suggested that several factors affect seismic velocities through soils and rocks including lithological, physical, and elastic properties of soils. Mirassi and Rahnema (2020) applied the propagation of seismic waves in homogenous half-space and layered soil media for deep cavity detection. Desper, et al. (2016) used the refraction method to estimate water table depth in a shallow unconfined aquifer in the Mulgrave River basin (Australia). Dhamiri and Zouaghi (2020) also applied near-surface geophysical surveys such as seismic refraction tomography (SRT), electrical resistivity tomography (ERT), and the time domain

electromagnetic (TDEM) for bedrock investigation and modeling for grain silos sites in western Saudi Arabia.

This study aims to investigate the subsurface geological features of the failed Chaqchaq dam reservoir to investigate the suitability of the ground condition of the dam, assessing bedrock strength using dynamic moduli of elasticity, mapping underground structures, and fractures.

Geological setting and hydrogeology

Geological setting

The Zagros orogenic belt resulted from the collision of the Arabian and Eurasian plates from the Cenozoic up to the present day (Fig. 2). The Zagros orogenic belt extends for almost 2000 km across Iran and Iraq, through Syria and southeastern Turkey. The tectonic evolution of the Zagros can be summarized as a series of Late Proterozoic, Permian, and Mesozoic rift events that were followed by the closure of the ancient continental margin leading to continental collision in the Cenozoic (Alavi, 2004 and 2007). Iraq can be divided into two main tectonic units, the Alpine geosyncline, and the Nubian-Arabian platform. The structure and structural development of Iraq is determined and strongly influenced by its position on the border between these two main Phanerozoic tectonic units of the Middle East (Buday and Jassim, 1987; Baban, 2001).

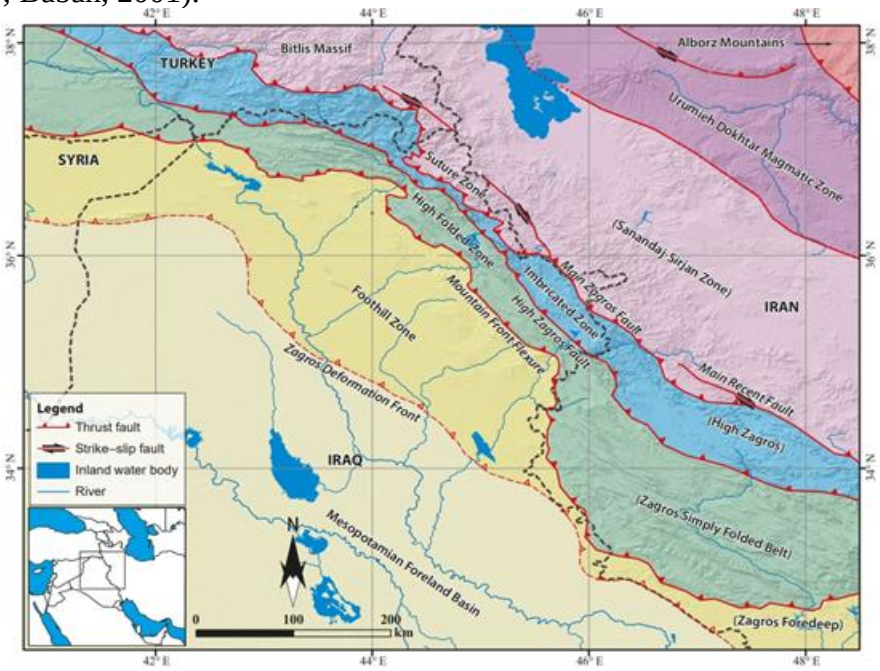

Fig. 2. Tectonic subdivision of the NW segment of the Zagros Fold-Thrust Belt (modified after Zebari, et al., 2019).

Tectonically, the studied area is located within the high folded zone, which lies in the Zakho -Sulaimani sub-zone of the northeastern part of Iraq within the Sulaimani-Sharazur Basin on the Sulaimani anticline. This anticline has been described for the first time as an independent structure by Al-Hakari (2011) (Figs.1 and 3). This anticline is around 2 km NW of Sulaimani City. It falls in two directions; its NW plunge began before the SE plunge of the Piramagrun anticline, forming an echelon with it, and its SW plunge began below Sulaimani City. It is a minor anticline that extends NW to SE and is separated from the Piramagrun by a short syncline.

Fig. 3. Geological structures around the Chaqchaq stream (Modified from Earth View, 2022).

The exposed geological units at and around the study area are represented by four formations, which begin with the Cretaceous succession including Qamchuqa, Kometan, Shiranish, and Tanjero formations as shown in (Fig. 4), in addition to the recent deposits observed in the study area.

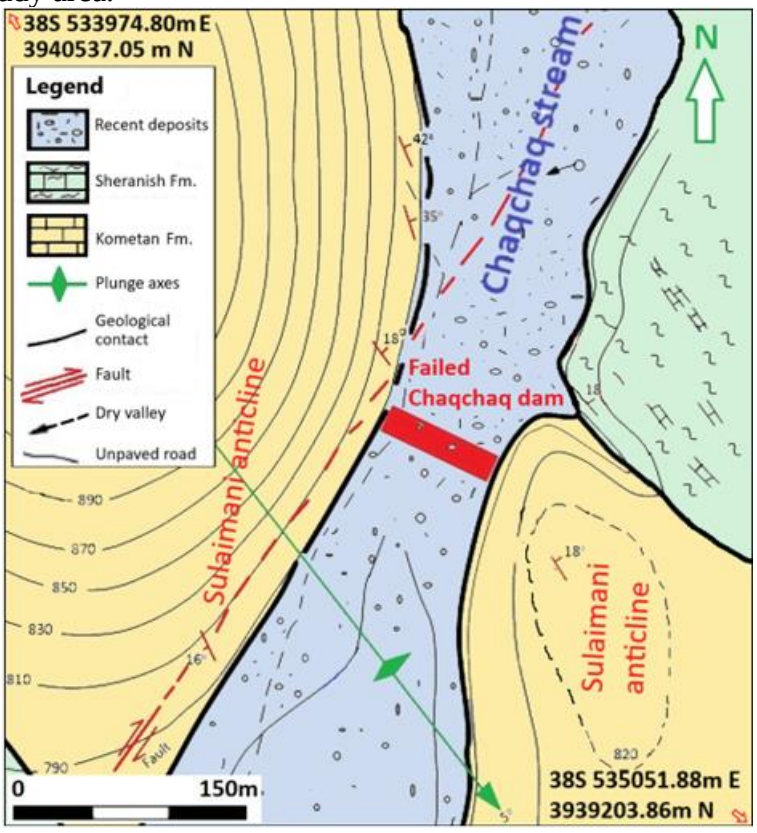

Fig. 4. Detailed structural features and geological formations of the study area (modified from FAO, 2001).

The lithology and stratigraphic successions of the study area belong to Kometan Formation. The lower contact of the Kometan Formation (Late Turonian- Early Campanian) is unconformable with Balambo and Qamchuqa Formations with a hiatus extended from Late Cenomanian to Early Turonian, and the upper contact is disconformable with Shiranish Formation (Buday, 1980; Al-Khafaf, 2005; Jassim and Goff, 2006). Lithologically, it consists of white-to-light-gray, hard, uniform, and medium-bedded limestone and chalky limestone (Al-Qayim, et al., 2012). The thickness of the Formation reaches 100-120 m (Karim, et al., 2008). The outcrop of this formation crops out in the plunge of Piramagrun and Sulaimani

anticlines as well as in the western part of Sulaimani City and the study area (Fig. 5 a and b). Tanjero Formation (Late Campanian to Middle-Late Maastrichtian) represents the thick Upper Cretaceous-Paleogene flysch sequence of the early Zagros Foreland Basin (Al-Qayim, 1993). Finally, the recent deposits and soil cover most parts of the study area (Fig. 5 b). Several geological and hydrogeological criteria may act as a hazard feature in the Chaqchaq stream basin. The geological factors include fault rapture and earthquake, mass movement, karstification, borrow materials, lithology, and rock mass, and hydrological factors include seepage, sedimentation, and flood.

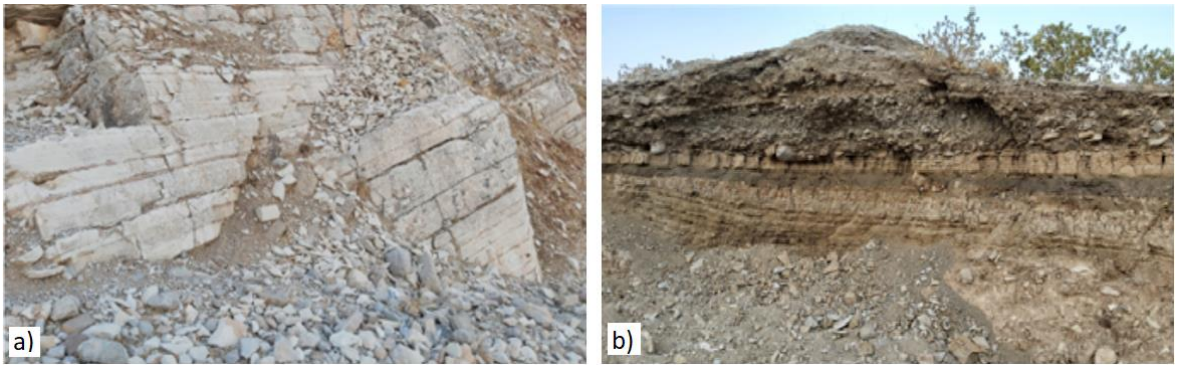

Fig. 5. a) Kometan Formation at the eastern side of Chaqchaq dam, and b) Recent deposit in the study area.

Hydrogeology

The study area's lowlands are confined to large valleys such as the Tanjero valley. Chaqchaq (Fig. 6) and Kani-pan are the two important streams in the region, they flow from the N and NW highs and have total lengths of 25.5 km and 14.6 km respectively (Khaleel, 2013). The Tanjero River, which flows about 13 Km southwest of the city center, is formed by the confluence of these two streams (near Kani-Goma village, about 7.5 km from the city center). Azmar anticlinorium, Piramagrun anticline, Sulaimani structure, and Sherkuzha anticline may be considered catchment areas for water sources that pour into the Chaqchaq stream. There are many deep and shallow wells near the study area. Some of them are called hand-wells that are shaved by hand. There is a borehole (water well monitoring) near the study area (772 m far from the Chaqchaq dam) with a depth of 400 m, an elevation of 780 m a.s.l, and a water level of 25.71 m, while the elevation of the study area ranges between 768-773 m. It means that the water table may be 14-17 m in the study area.

Fig. 6. Location of the Fifteen seismic refraction traverses in the study area (Google Earth, 2022).

Seismic Refraction Analysis

Data acquisition

Seismic fieldwork is one of the most important three phases of any seismic survey. It must be executed with safe and high accuracy. If there is any mistake in fieldwork measurements, it will be reflected in the other phases of the survey. Before starting the fieldwork, attention must be taken to how can investigation site be selected, the target of the survey, some knowledge about the geology of the area, expecting seismic velocity contrast between the geological boundaries of interest to choose the proper instruments and layout of the survey, type of survey; the number of the traverses covering the area of study, two or three-dimensional survey, designing spread and layout, number of the geophones and spacing between them, type of energy source, ...etc., (Reynolds, 2011).

Field data acquisition, processing, and interpretation of seismic refraction data are usually fast, simple, and low-cost. Two people can conduct the survey, and in case of using explosives or a weight drop, a third person may be required. The data are acquired by applying a source of seismic energy at several locations within and outside the spread of receivers. The processing and interpretation are performed using a PC-based simple interactive software. The final product of refraction surveys is a layered depth section including information on layer geometry and seismic velocities within the layers (Palmer, 1986).

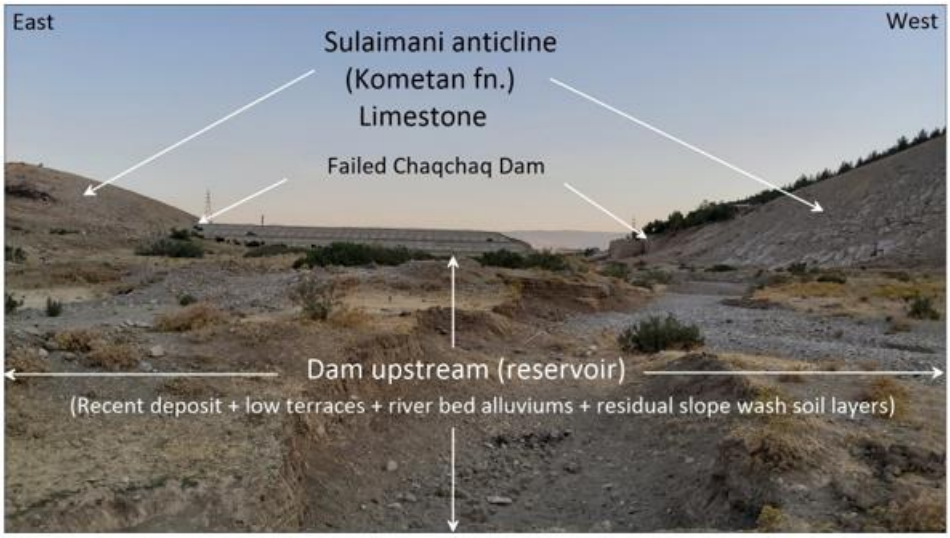

Fig. 7. Upstream (reservoir) side of the failed Chaqchaq dam (study area).

The field survey measurements are conducted on the upstream (reservoir) side of the dam. Seismic refraction data are collected from fifteen parallel traverses, whose trends are in a South-North direction (Figs. 6, 7, and 8) using a modern computerized Geode 24-channel (24 Geophones) signal improved seismograph of Geometrics Inc.

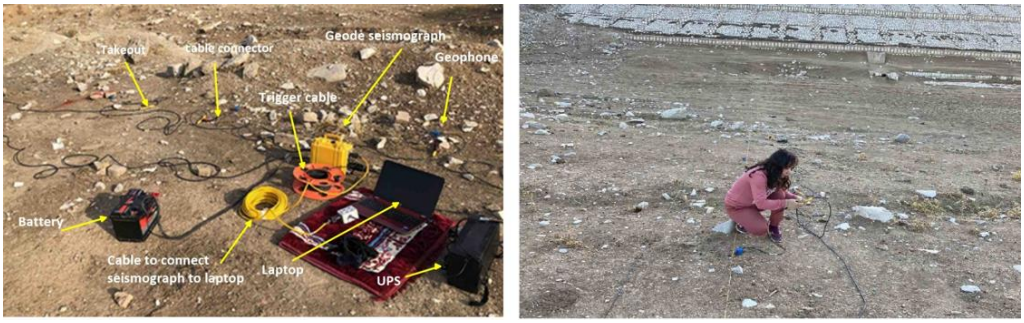

Fig. 8. Photos of the fieldwork showing the connection between the Geode and accessories of the seismic refraction survey.

Three shot-points on three positions of the lines (each traverse consists of two lines) were applied using a 10 LB sledgehammer as a source of energy at the left, center, and right sides of seismic survey lines, which means six shot-points were used for each traverse (Fig.

9). The total length for each traverse (the two lines) was 230 m. The spacing between the geophones on each traverse was 5 m, while the spacing between the traverse was 10 m except the spacing between traverses Tr-14 and Tr-15 which was 20 m because the area between these two traverses consists of a lot of gravel, sand, and rock fragments that make the penetrating of the geophones difficult and sometimes impossible.

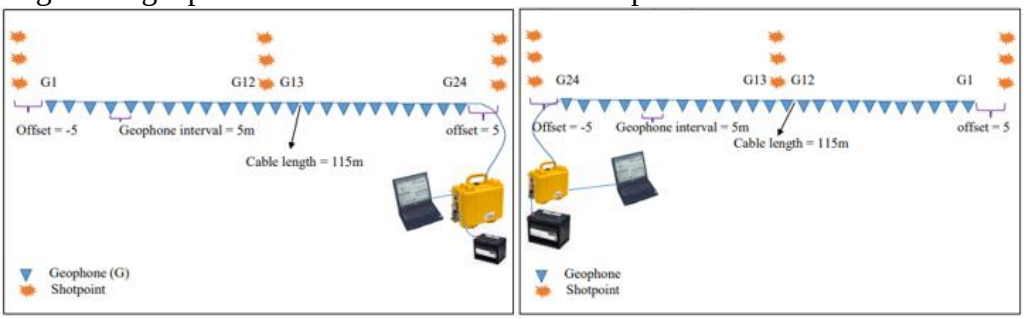

Fig. 9. Data acquisition layout of seismic refraction.

Data processing

Seismic data processing is done using SeisImager/2D software (Geometrics and OYO corporation). This software consists of many modules (programs), such as Pickwin and Plotrefa modules. Pick win is used for pick first breaks, and Plotrefa performs seismic refraction analysis, creates a travel-time curve, calculates the velocities for the layers, performs tomography, inversion, and modeling, and draws the results section. This software had Quality Control which is important for checking data.

The main goal of seismic data processing is to increase the signal-to-noise ratio and to create a perfect seismic section. The following steps for data processing are applied; editing the geometry for all shots of the traverse, choosing a proper filter to remove the noises and enhance the signal, and picking the first arrival of the P-wave for all of the recorded data for every shooting. To accomplish the precise first arrival picking, the amplitude of each trace was manually adjusted (Fig. 10). Then the result was saved in a file having an extension of (.vs).

After obtaining the travel time-distance curve, it was saved in a file having an extension of (.vs) for each seismic line. These curves were rectified and reviewed to ensure that the P-wave velocity was accurately estimated. The raytracing tab is used to calculate the root mean square error (RMSE) percentage error, and as this error is small, the result got better. After that, the data are ready to perform the tomography inversion automatically and manually for generating the tomographic inversion model and creating the forward modeling. Finally, they inverted travel time data to a two-dimensional velocity section. The results were saved in a file in an ASCII columnar XYZ format or text format for import into third-party graphics programs such as Golden Grapher or Surfer software.

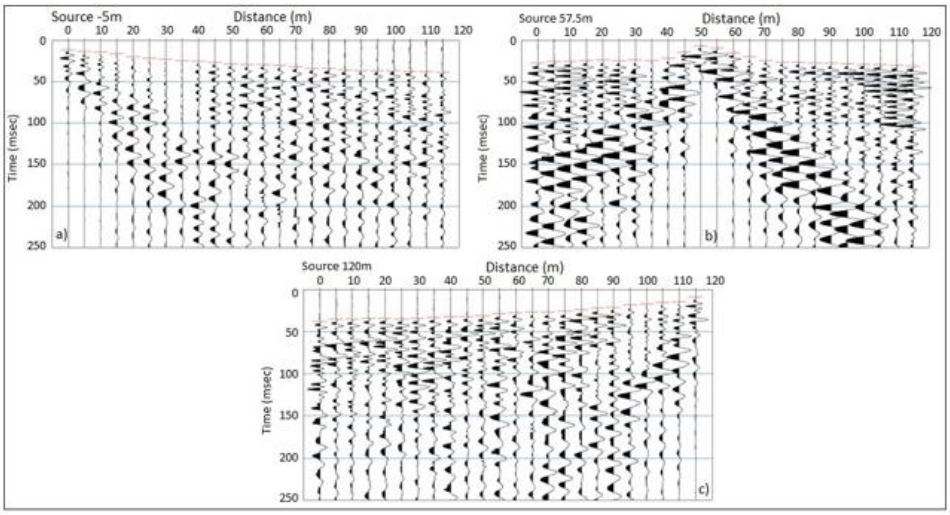

Fig. 10. The first break picking for Tr-1 traverse; a) Forward shot, b) Center shot and c) Reverse shot.

The shear wave velocity is the dominant parameter influencing changes in Rayleigh wave phase velocity. It has been shown that Rayleigh wave phase velocity data can be inverted and used to generate reliable corresponding shear wave data (Miller and Park, 1999). Shear wave velocity for the first, second, and third layers are calculated from SeisImager/2D software. The first arrival travel times of the recorded data for (S-waves) are picked manually as shown in Fig. (11) to calculate Vs from the time-distance curve for each layer.

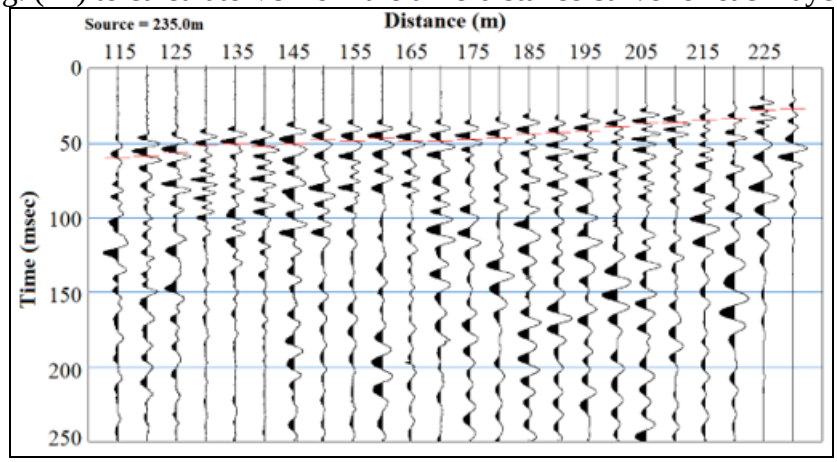

Fig. 11. Determined secondary wave velocity (S-Wave) for Tr-1 traverse using Picwin SeisImager/2D software.

Interpretation

Seismic Refraction Tomography interpretation

The automated and manual picking of first break arrival is used for the Tr-3 traverse as shown in Fig. (12 a) to get rapid and reliable results for picking the first breaks. For shot-to-shot coherence, add geometry, and remove noisy data with robust filtering simultaneously. The generated travel time curve of the traverse is shown in Fig. (12 b). The RMSE value of the traverse was 1.9 ms.

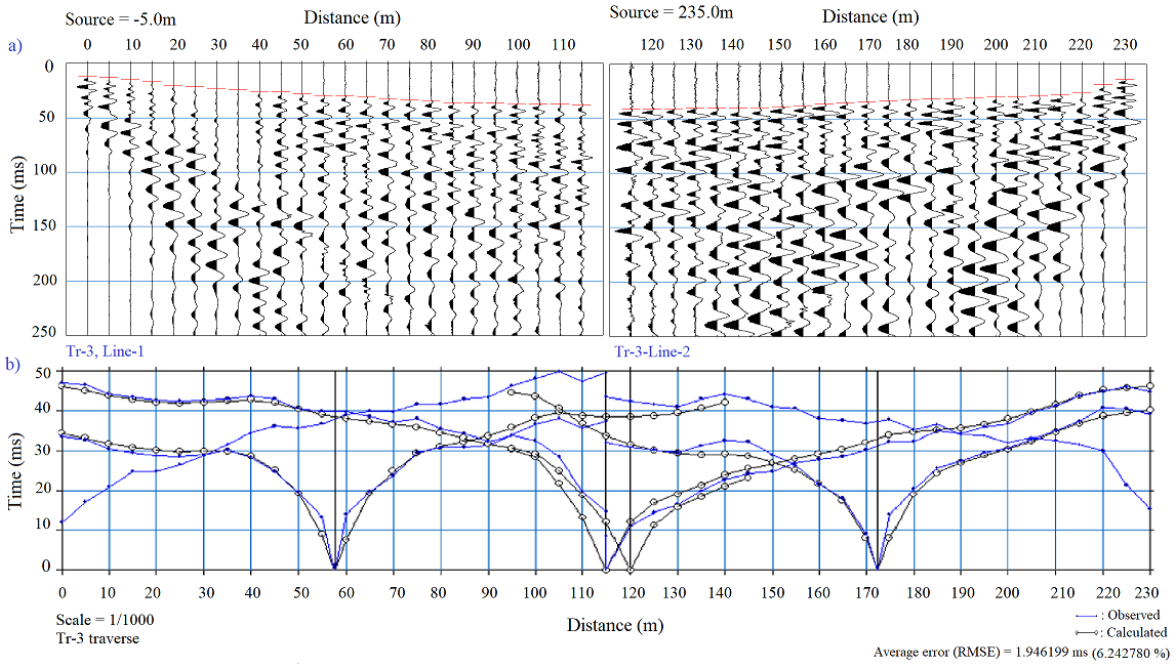

Fig. 12. SRT processing for Tr-3 traverse; a) First break Picking, b) Travel time (Time-Distance) curve.

For all fifteen traverses, the seismic tomography inversion section consists of a 15-color scale that is constructed according to the velocity contrast between layers. The three geological layers model for 2D seismic velocity sections is generated according to the lithological changes in the area under study. The Seismic refraction tomography and three-

layer geological model sections of the Tr-3 traverse are shown in Fig. (13 a and b). It seems that the first layer (pink color) consists of the soil, approximately regular and flat, while the second layer (red and orange colors) is composed of rock fragments. It is appearing that there are some small changes and undulation within the second layer. The surface of the third layer (yellow color) is the top of the fractured limestone of the Kometan Formation. It can recognize several features within the Kometan Formation (models of yellow to blue colors). The topography of the Kometan limestone is irregular due to weathering, fracture, and erosion; as a result of tectonic movement and stress, the area collapsed and it filled with recent deposits or may be decomposition occurs by water in the fracture of this layer, and by karstification. There are three uplifts at distances of 30-50 m, 125-140 m, and 150-180 m. There are four dispersions at distances 0-30 m, 50-127 m, 140-150 m, and 180-220 m that are visible in Fig. (13 a). All depressions are filled with sediments of recent deposits. The light blue color expresses the hard and compact limestone of the Kometan Formation. Figure (13 b) shows the three lithological layers model for 2D seismic velocity. Additionally, this traverse reveals that the region is composed of three geological layers. The first (soil) layer is generally regular and flat, having a thickness of (1.04-2.81 m) and a velocity is 411 m/s. The top of the second layer has typically many lateral changes, and consists of rock fragments with a thickness ranging between (8.51-12.66 m) and a velocity are 1294 m/s. The third layer has a generally irregular surface as the above traverses, it lies at a depth ranging from (9.6-15.5 m) and the velocity is greater than 4344 m/s.

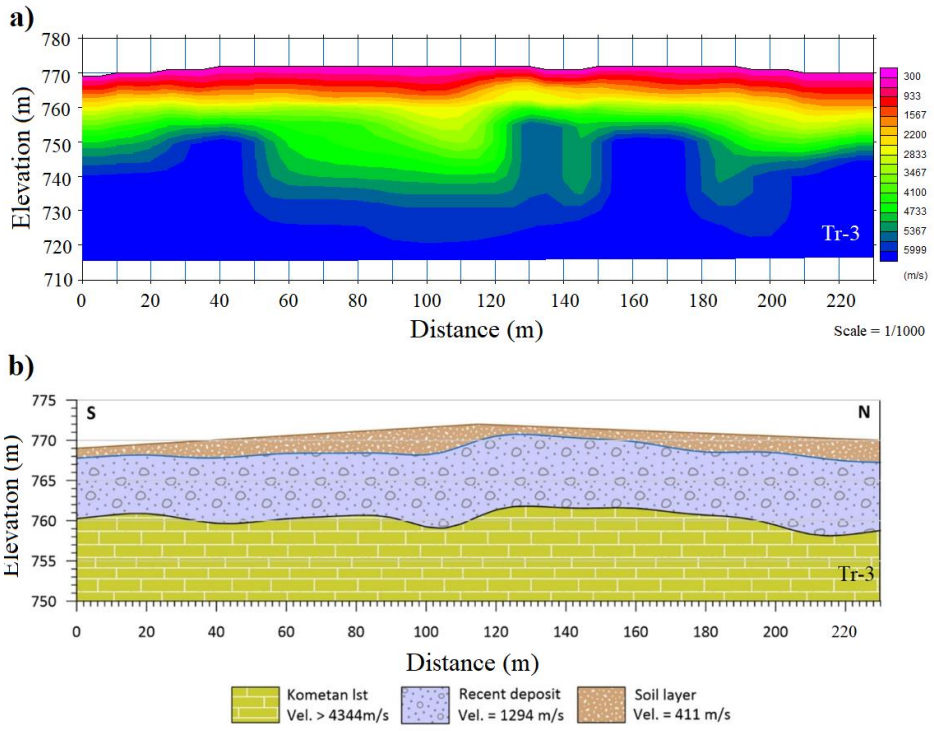

Fig. 13. a) Seismic refraction tomography (SRT) section. b) the 2D velocity layer model and cross-section of the subsurface layers resulting from tomography inversion for Tr-3 traverse.

The Seismic refraction tomography section of the Tr-6 traverse is shown in Fig. (14 a). The first (soil) layer (pink color) is approximately regular with a flat elevation ranging between 769-771 m. The second layer (red and orange colors) consists of rock fragments. The surface of the third layer (yellow color) is the top of the fractured limestone. Within this layer, numerous features and small lateral variations are detected. At the beginning and end of this traverse, there are two depressions approximately between distances 0-140 m and 195-230 m. There is an uplift between the distance 140-195 m. The light blue color expresses the approximately flat hard and compact limestone of the Kometan Formation. Figure (14 b) displays three lithological layers model for 2D seismic velocity. The first (soil) layer has a thickness of (0.95-2.13m) and a velocity of 421 m/s. The second layer consists of rock fragments having a thickness range between (7.34-10.64 m) and a velocity of 1268 m/s. The third layer, which has an irregular surface and is composed of fracture limestone of the

Kometan Formation, is located at depth ranges between (8.3-12.8 m) and has a velocity greater than 4596 m/s.

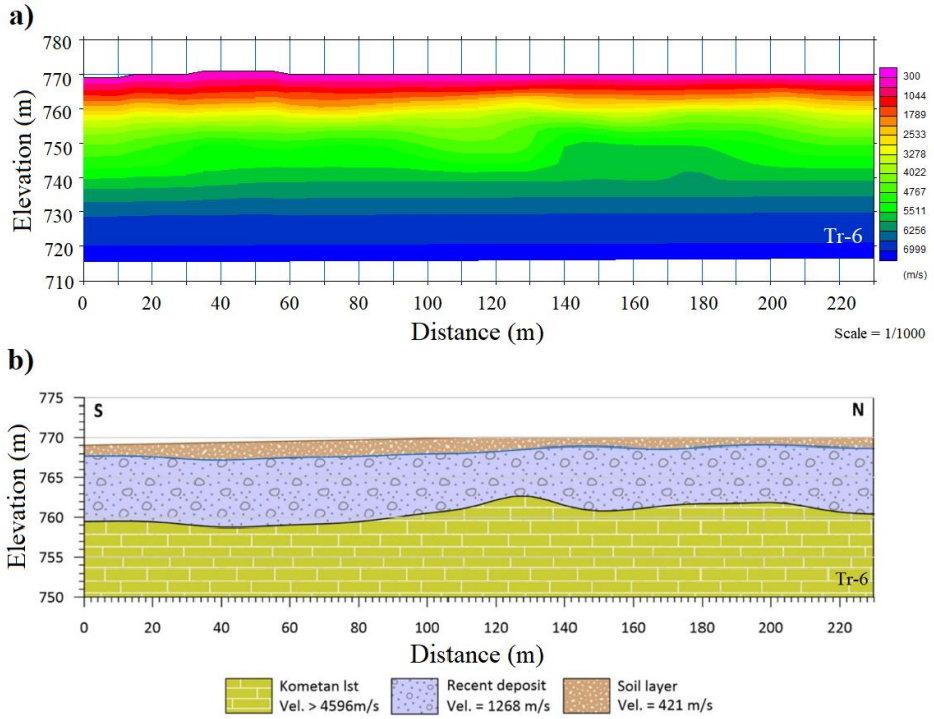

Fig. 14. a) Seismic refraction tomography (SRT) section. b) the 2D velocity layer model and cross-section of the subsurface layers resulting from tomography inversion for Tr-6 traverse.

In the Tr-11 traverse (Fig. 15) the same layers and features as mentioned in the above traverses with different locations and elevations are shown. There are two uplifts at the center and northern parts of the traverses between the distance 60-120 m and 190-230 m. There are two depressions at the south part and another between the distances 0-80 m and 120-200 m. The Seismic refraction tomography and three-layer geological model sections of the Tr-15 traverse shown in Fig. (16) represent a wide and large depression within the Kometan limestone Formation between the distances 110 to 190 m.

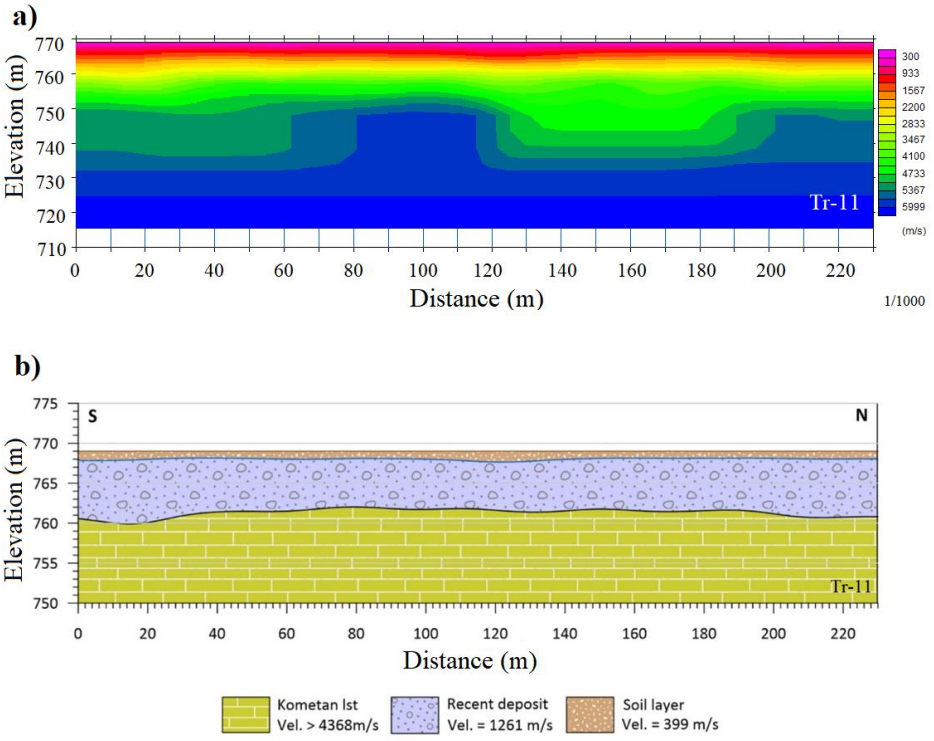

Fig. 15. a) Seismic refraction tomography (SRT) section. b) the 2D velocity layer model and cross-section of the subsurface layers resulting from tomography inversion for Tr-11 traverse.

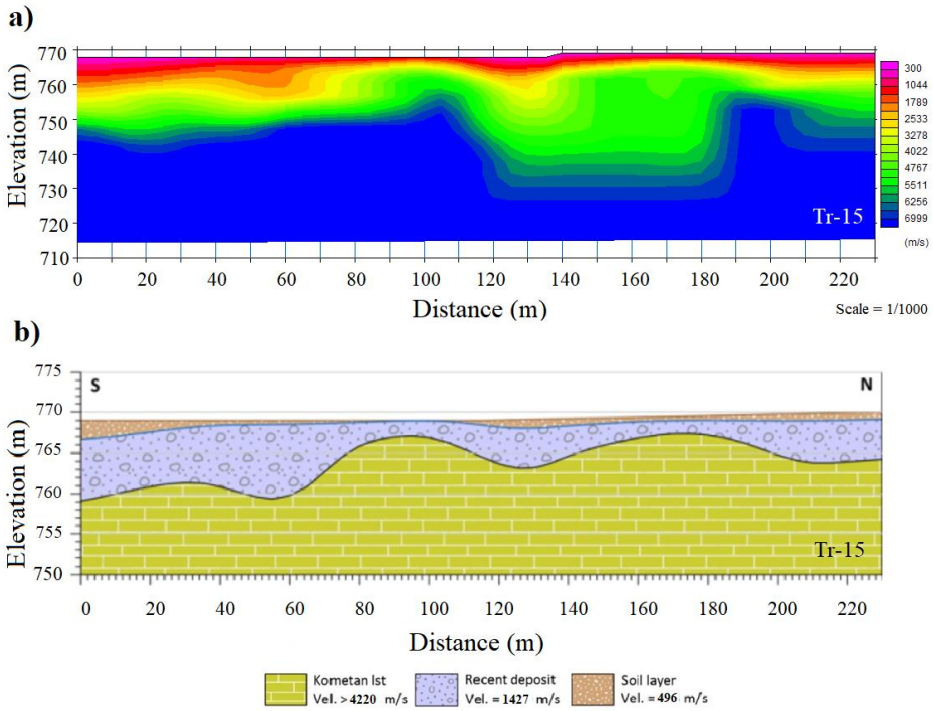

Fig. 16. a) Seismic refraction tomography (SRT) section. b) the 2D velocity layer model and cross-section of the subsurface layers resulting from tomography inversion for Tr-15 traverse.

All SRT traverses are summarized and illustrated in (Table 1) below: -

Table 1. Velocities, thickness, and depth for five traverses were calculated by seismic refraction tomography software.

Traverses	Average Layers Velocities			Layer and Depth Ranges		
				Thicknesses		Depth
	V1 (m/sec)	V2 (m/sec)	V3 (m/sec)	Z1 (m)	Z2 (m)	H (m.)
Tr-1	440	1351	5108	0.96-2.45	6.47-11.20	7.4-13.7
Tr-2	352	1139	4387	0.67-2.29	7.07-11.10	7.7-13.4
Tr-3	411	1294	4344	1.04-2.81	8.51-12.66	9.6-15.5
Tr-4	428	1221	4547	0.63-3.10	6.39-13.11	7.0-16.2
Tr-5	417	1276	4519	1.03-2.83	7.73-10.66	8.8-13.5
Tr-6	421	1268	4596	0.95-2.13	7.34-10.64	8.3-12.8
Tr-7	438	1387	4508	0.88-2.09	6.04-9.96	6.9-12.0
Tr-8	418	1240	4610	0.91-2.19	7.51-10.91	8.4-13.1
Tr-9	456	1335	4426	0.93-2.10	7.47-9.29	8.4-11.4
Tr-10	427	1361	4514	1.05-1.97	7.13-10.24	8.2-12.2
Tr-11	399	1261	4368	0.86-1.3	6.98-8.96	7.8-10.3
Tr-12	416	1322	4219	0.27-0.98	4.18-7.53	4.5-8.5
Tr-13	424	1396	4660	0.49-1.20	5.14-7.89	5.6-9.1
Tr-14	516	1363	4485	0.31-1.16	4.39-8.40	4.7-9.6
Tr-15	496	1427	4220	0.05-2.36	1.93-9.89	2.0-12.3

Geological mapping of subsurface layers

Finally, the depth and thickness maps for the main three geological layers (Soil, recent deposits, and Kometan formation) are constructed from obtained results.

A three-dimensional map of the top of the first layer (Fig. 17) shows that the northeast part is the highest and the southwest is the lowest part (the two biggest depressions) of the study area. The maximum elevation value reaches 772.8 m in the eastern part while the minimum elevation value is 767.8 m observed in the southwestern part. This means that the direction of water flow upstream is toward the west and exactly toward the southwestern part of the area. This phenomenon is emphasized by a constructed watershed map of the layer (Fig. 18).

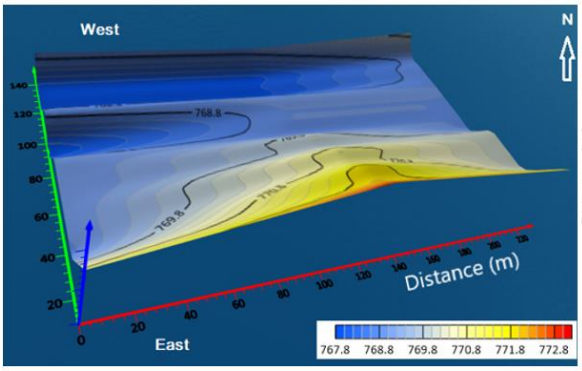

Fig. 17. Three-dimensional contour map of the top of the first layer

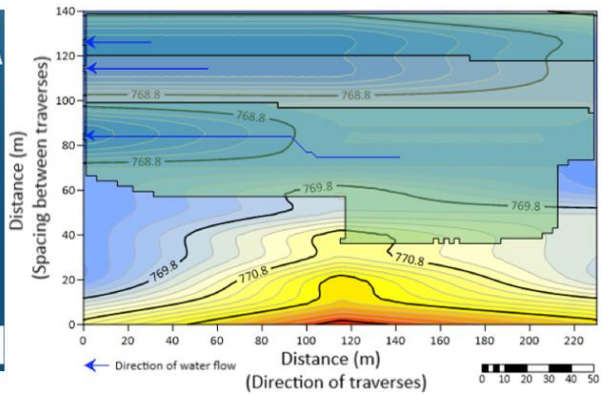

Fig. 18. Two-dimensional contour map, watershed, and water flow of the top of the first layer.

A three-dimensional map of the top of the second layer (Fig. 19) showing also that the surface of this layer is irregular and the highest part lies in the northeast part while the lowest parts (the two biggest elongated depressions) are located at the southwest of the study area. The maximum elevation value reaches 771.8 m in the eastern part while the minimum elevation value is 766.3 m observed in the southwestern part. This means that the direction of water flow upstream is toward the west and the southwestern parts of the area. These phenomena, as in the first layer, are emphasized by a constructed watershed map of the layer (Fig. 20).

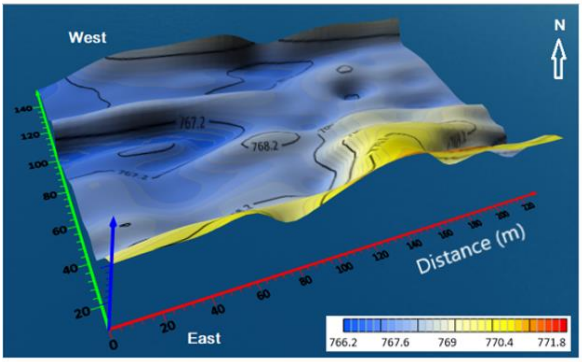

Fig. 19. Three-dimensional contour map of the top of the second layer.

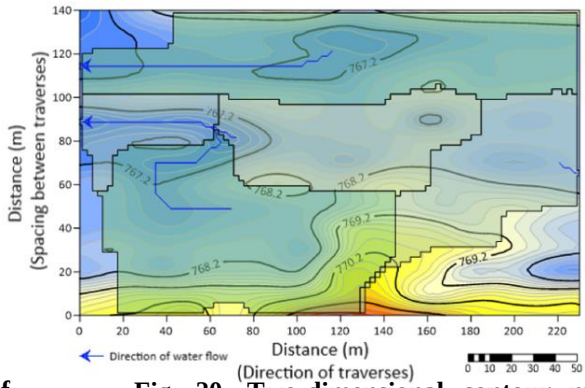

Fig. 20. Two-dimensional contour map, watershed, and water flow of the top of the

The three-dimensional map of the top of the third layer (Fig. 21) shows that the surface of this layer is irregular, weathered, and fractured containing several high and low features in different positions of the map with different elevations. The high features are concentrated in the north from west to east while the low features are concentrated in the south and some of the small and deep features at the extreme of north and northeast. These low features may be reflected in the presence of voids or cavities filled with sediment and water. The direction of water flow upstream is toward the southern part of the area. This phenomenon as in the first and second layers is emphasized by a constructed watershed map of the layer (Fig. 22).

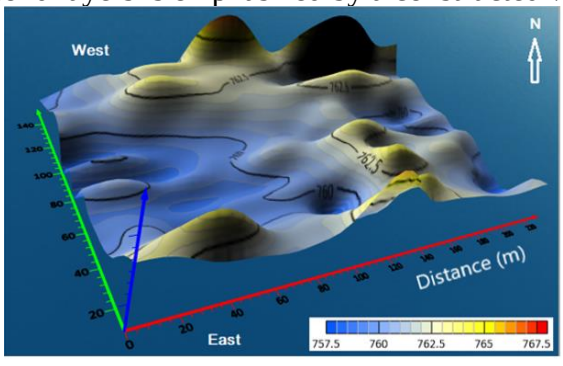

Fig. 21. Three-dimensional contour map of the top of the third layer.

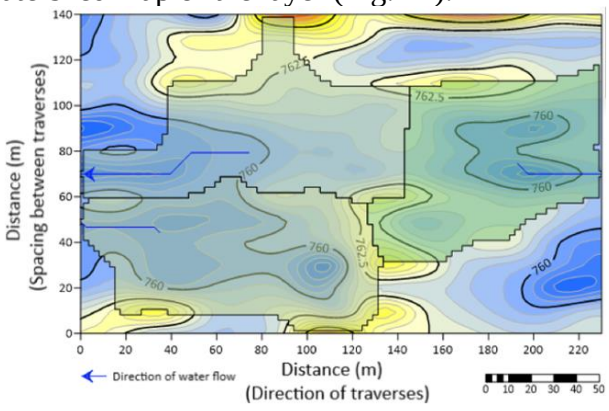

Fig .22. Two-dimensional contour map, watershed, and water flow of the top of the third layer.

Finally, the isopach (thickness) three-dimensional maps of the first and second layers are constructed. The isopach map of the first layer (Fig. 23) shows that the thickness of the layer differs from one place to another. The layer is thickened at the central part of the area (more than 3.6 m, while the layer is thinning at the north, northwest, southwest, and southeast. There are several high and low features within this layer. The isopach map of the second layer (Fig. 24) is thicker than the first one and in general, the thickness of the layer ranges between 6 to 9 m except at the extreme of the northeast and center of the eastern part where it reaches more than 10 m and several high and low features are visible on the map.

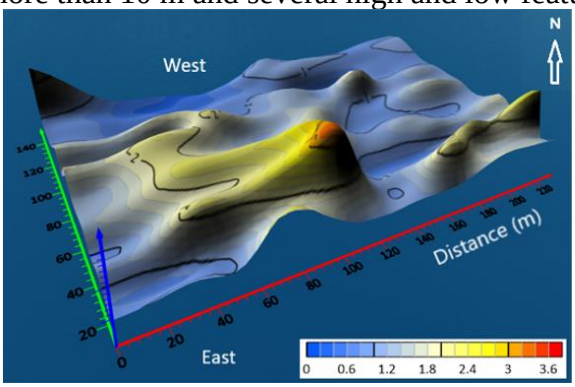

Fig. 23. Three-dimensional contour map of the thickness of the first layer

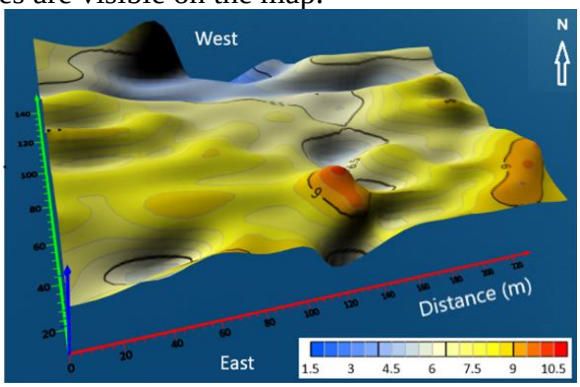

Fig. 24. Three-dimensional contour map of the thickness of the second layer.

Dynamic moduli of elasticity result from seismic refraction

Seismic refraction is applied to solve engineering problems by calculating the dynamic moduli of elasticity. Seismic refraction is inexpensive, needs less time, and provides regional information. According to seismic velocity results, many engineering dynamic moduli are determined, which are extremely beneficial for construction. Discovering subsurface dynamic moduli of elasticity requires direct measurements, with high resolution, which provide local information, and need more cost and time which is sometimes partial significance. So, in the present study, the calculations of Vp and Vs will lead to determining Poisson's ratio (σ), Elastic modulus (E), Shear (Rigidity) modulus (μ), Bulk modulus (B) and Compressibility (K), through the parameters of the dynamic elasticity equations shown in the following (Table 2).

Table 2. Dynamic moduli of elasticity equations.

Rock parameters	Equation	Reference
Poisson's Ratio (σ)	$\sigma = \frac{Vp^2 - 2Vs^2}{2(Vp^2 - Vs^2)}$	(Andrea, et al., 1965; Potter, and Fottinek, 1997)
Elastic (Young's) modulus (E)	$E = 2\rho Vs^2(1+\sigma)$	
Shear modulus (G)	$G = \rho Vs^2$	
Bulk modulus (B)	$B = \rho Vp^2 - \frac{4}{3}\mu$	
Compressibility (K)	$K = \frac{1}{B}$	
General density (ρ)	ρ = Vo + 0.002 * Vp	Tezcan, et. al., (2006)

Vp is the propagation velocity of the compressional waves, Vs is the propagation velocity of the shear waves, and Vo is the reference unit of weight values.

From the analysis of data, the velocities and densities are determined and then substituted in the above relevant equations for the geotechnical engineering parameters (dynamic moduli of elasticity) calculations for the first, second, and third layers as shown in Table (3).

Table 3. The calculated geotechnical engineering parameters along Seismic Refraction Traverses.

Traverses	Layers	P-Velocity	S-Velocity	Poisson's Ratio	Density	Elastic modulus	Shear modulus	Bulk modulus	Compressibility
		Vp (m/sec.)	Vs (m/sec.)	σ	ρ (kg/m^3)	E (N/m^2 x 10^8)	μ (N/m^2 x 10^8)	B (N/m^2 x 10^8)	K (m^2/N)
Tr-1	Layer 1	440	187	0.39	1688	1.64	0.59	3.27	0.31
	Layer 2	1350	710	0.31	1870	24.68	9.43	34.08	0.03
	Layer 3	5108	3004	0.24	2622	584.64	236.57	684.02	0.001
Tr-2	Layer 1	352	160	0.37	1670	1.17	0.43	2.07	0.48
	Layer 2	1139	570	0.33	1828	15.83	5.94	23.71	0.04
	Layer 3	4387	2589	0.23	2477	409.43	166.06	476.79	0.002
Tr-3	Layer 1	411	179	0.38	1682	1.491	0.54	2.84	0.35
	Layer 2	1294	650	0.33	1859	20.91	7.85	31.12	0.03
	Layer 3	4344	2555	0.24	2469	398.25	161.16	465.87	0.002
Tr-4	Layer 1	428	200	0.36	1686	1.83	0.67	3.09	0.32
	Layer 2	1221	642	0.3	1844	19.9	7.6	27.49	0.04
	Layer 3	4547	2641	0.25	2509	435.98	175.03	518.82	0.002
Tr-5	Layer 1	417	178	0.39	1683	1.48	0.53	2.93	0.34
	Layer 2	1276	671	0.31	1855	21.87	8.35	30.21	0.033
	Layer 3	4519	2658	0.24	2504	437.11	176.89	511.31	0.002
Tr-6	Layer 1	421	200	0.35	1684	1.82	0.67	2.99	0.33
	Layer 2	1268	647	0.32	1854	20.55	7.76	29.8	0.03
	Layer 3	4596	2684	0.24	2519	450.52	181.48	532.14	0.002
Tr-7	Layer1	438	198	0.37	1688	1.81	0.66	3.24	0.31
	Layer 2	1387	701	0.33	1877	24.51	9.23	36.12	0.03
	Layer 3	4508	2651	0.24	2502	434.48	175.81	508.38	0.002
Tr-8	Layer1	418	179	0.39	1684	1.5	0.54	2.94	0.34
	Layer 2	1240	652	0.31	1848	20.57	7.86	28.41	0.04
	Layer 3	4610	2711	0.24	2522	458.08	185.35	535.98	0.002
Tr-9	Layer 1	456	217	0.35	1691	2.16	0.8	3.52	0.28
	Layer 2	1335	702	0.31	1867	24.09	9.2	33.27	0.03
	Layer 3	4426	2539	0.25	2485	402.05	160.21	486.84	0.002
Tr-10	Layer 1	427	193	0.37	1685	1.72	0.63	3.07	0.33
	Layer 2	1361	716	0.31	1872	25.12	9.6	34.68	0.03
	Layer 3	4514	2665	0.23	2503	438.16	177.75	509.98	0.002
Tr-11	Layer 1	399	185	0.36	1680	1.57	0.57	2.67	0.37
	Layer 2	1261	653	0.32	1852	20.8	7.9	29.45	0.03
	Layer 3	4368	2563	0.24	2474	402.15	162.49	471.95	0.002
Tr-12	Layer 1	416	198	0.35	1683	1.79	0.66	2.91	0.34
	Layer 2	1326	697	0.31	1865	23.72	9.06	32.8	0.03
	Layer 3	4219	2481	0.24	2444	371.76	150.42	434.1	0.002
Tr-13	Layer 1	424	166	0.41	1685	1.3	0.46	3.03	0.33
	Layer 2	1396	715	0.32	1879	25.4	9.61	36.62	0.03
	Layer 3	4660	2751	0.23	2532	472.36	191.62	549.84	0.002
Tr-14	Layer 1	516	187	0.42	1703	1.7	0.6	4.53	0.22
	Layer 2	1363	686	0.33	1873	23.45	8.81	34.79	0.03
	Layer 3	4485	2638	0.24	2497	429.39	173.77	502.28	0.002
Tr-15	Layer 1	496	231	0.36	1699	2.47	0.91	4.18	0.24
	Layer 2	1427	762	0.3	1885	28.47	10.95	38.39	0.03
	Layer 3	4220	2472	0.24	2444	370.02	149.35	435.24	0.002

Discussion

Several factors, such as weathering, fractures, cavities, faults, water content, and porosity, affect SRT results, although their sensitivity may differ. The geophysical results are compared with available boreholes and outcrops which allowed the geophysical data interpretation to be validated. According to the SRT method results, it seems that this region consists of three layers, soil, rock fragments, and limestone (Kometan Formation) respectively. The Vp of the first layer ranges between 352 m/s to 516 m/s and the Vs ranges between 160 m/s to 231 m/s with the thickness ranging between 0.05-3.10 m, while for the second layer the Vp ranges between 1139 m/s to 1427 m/s and the Vs ranges between 570 m/s to 762m/s with the thickness ranging between 1.93-13.11m, and the third layer is specified as a consolidated and cohesive limestone of Kometan Formation with the primary velocities ranging between 4219-5108 m/s in a depth ranging between 2.0-16.2 m and the Vs ranges between 2472 m/s to 3004 m/s.

The presence of surface water in recent deposits at depths 2.0-14 m may cause soil and rock fragments to liquefy. The topography of the Kometan limestone is irregular due to weathering, fracture, faults, cavities, collapse, and erosion; and as a result of tectonic movement and stress, the area, collapsed and was filled with sediments of recent deposits, or maybe decomposed by water in the fractured limestone, and karstification occurred. The topography of the bedrock of one side in the west direction is shallower than the east and central parts, this is the result of the presence of the slope as well as the erosion process during the seasonal stream water which leads to transgressed the recent sediment of the first layer especially along of side west area. Based on the results of this study and according to UFC (2008), seismic velocities for weathered rocks range between 609.600-3048.000 m/s. Presence of all these weathering, and fracture features within the top of the Kometan Fn. layer means this part of the Kometan Formation is unsuitable of constructed the dam the third layer of bedrock consists of rock from the Kometan Formation, which can be considered as the base of the dam foundation.

Based on the estimated geotechnical parameters from Vp and Vs and measured density, Poisson's ratio ranges between 0.35-0.42 for the first layer is characterized by a relatively high Poisson's ratio meaning that the rocks can fracture easily and indicating incompetent to fairly competent soil and the elastic modulus ranges between 1.17 $N/m^2 \times 10^8$ to 2.47 $N/m^2 \times 10^8$ and the shear (rigidity) modulus ranges between 0.43 $N/m^2 \times 10^8$ to 0.90 $N/m^2 \times 10^8$ and bulk modulus ranges between 2.07 $N/m^2 \times 10^8$ to 4.53 $N/m^2 \times 10^8$. The inverse values of the bulk modulus give the compressibility ranges between 0.22 to 0.48 m^2/N. This result will indicate that the first layer is weak and fissured and subjected to sinkholes buried with recent sediments. The Vp of the second layer increasing ranges from 1139 m/s to 1427 m/s will lead to a decrease in Passion's ratio range from 0.30 to 0.34 indicating the rocks are harder to fracture than the first layer because Poisson's ratio changes from layer to layer and reflected fairly to moderate competent soil/rock. The elastic modulus ranges between 15.83 $N/m^2 \times 10^8$ to 28.48 $N/m^2 \times 10^8$ and the shear modulus is 5.94 $N/m^2 \times 10^8$ to 10.95 $N/m^2 \times 10^8$ and the bulk modulus ranges between 23.71 $N/m^2 \times 10^8$ to 38.39 $N/m^2 \times 10^8$, and its compressibility ranges between 0.03 to 0.04 m^2/N. The elasticity moduli reveal low to moderate values of elasticity, which reflects that this layer is composed of unconsolidated recent sediments subjected to weathering process due to the flowing of water in seasonal raining up to Tr-10 traverse leading to evaluate moderate elasticity values, whereas from Tr13 to Tr-15 traverse, the stream is formed due to the effect of water flow through the collapsed part of the constructed dam which leads to removing the recent sediments and appearing of bedrock covered by clastic debris covers and making the moderate elasticity values. The results of the elasticity moduli of the third layer show that the lower layer is characterized by good competent rock quality according to Table (4) with the value of Poisson's ratio ranging between 0.23-0.25 is characterized by relatively low Poisson's ratio indicating the rocks are harder to fracture than the first and second layer. The elastic modulus ranges between 370 $N/m^2 \times 10^8$ to 585 $N/m^2 \times 10^8$ and the rigidity 149.34 $N/m^2 \times 10^8$ to 236.57 $N/m^2 \times 10^8$ and the bulk modulus ranges between 434.99 $N/m^2 \times 10^8$ to 684.02 $N/m^2 \times 10^8$, and its compressibility ranges between 0.001 to 0.002 m^2/N. The Elastic modulus and shear (rigidity) modulus as well as bulk modulus values are increased by increasing velocities as well as densities; and when the bulk modulus is increased, the compressibility is decreased because of the (inverse proportionality) and the layers become more competent characteristic due to compaction process.

Table 4. Classification of soil's competent according to Poisson's ratio, (Khalil, and Hanafy, 2008).

Soil description	Incompetent to slightly competent	Fairly to moderately competent	Competent material	Very highly competent materials
Poisson's Ratio (σ)	0.41-o.49	0.35-0.27	0.25-0.16	0.12-0.03

The results would show that the relationship between Vp and Vs of the first, second, and third layers is linear because the velocity increases with depth, whereas the relationship between the elastic modulus is considered a function of Vp, and there is a direct proportion

between them. Shear modulus is considered a function of the Vp, and it is directly proportional to shear modulus, bulk modulus is directly proportional to velocity. The relationships between the Poisson's ratio and the ratios of Vs/Vp for the first layer and Vs/Vp for the second layer are pointed as inverse relationships. This means that increasing Poisson's ratios reduces the ratios of Vs/Vp and this will increase the brittleness of materials. The relationship between Vp for the first and second layers with compressibility is inversely proportional. The inverse relationship is deduced between the ratio of B/μ and the ratio of Vs/Vp. This relationship is a very important one from an engineering point of view where it can be used to separate the weak zone areas from the strong zones (Dutta, 1984).

The result of (Fig.17) shows that the top of the first layer, the northeast part, is the highest, and the southwest is the lowest part (the two biggest depressions) of the study area. While the surface of the second layer (Fig. 19) is irregular and the highest part lies at the northeast part while the lowest parts (the two biggest elongated depressions) are located at the southwest of the study area. The surface of the third layer (Fig. 21) is irregular, weathered, and fractured containing several high and low features in different positions of the map with different elevations. The high features are concentrated in the north from west to east, while the low features are concentrated in the south and they are some of the small and deep features at the extreme of the north and northeast. These low features may be reflected in the presence of voids or cavities filled with sediment and water. As a result, the direction of the water flow upstream (Figs. 18, 20, and 22) is toward the west and exactly toward the southwestern part of the area, which causes stress at the wall of the dam causing the failure of the dam wall in this region. Petaccia (2016) reported that the first dam collapsed in Italy caused by foundation instability combined with changes in the construction methodology and 1928 the St Francis dam (California, USA) failed because of the poor quality of the bedrock.

The results are very important for redesigning the collapsed dam by reconstructing the base of the dam to the suitable depth of the Kometan Formation for at least 10-45 m by concrete and the dam beside the spillway must include three automatic gates along the dam for controlling the amount of water releasing to the Qliasan stream in the summer season, and the shoulder of the dam will be inter tied with an adjacent rock to laterally 5 m length at both side of the dam. This design will stand in front of the hydrostatic pressure of the reservoir water in the lake subjected to the dam in case of filling it with water. By this design, the dam will be on the safe side in case of any unexpected natural feature, especially in case of flooding the spillway and the gates will control the side effect of the flood and will also control the permanent existence of water in the lake and the Qliasan stream in all seasons.

Conclusion

There are three layers in the studied region; the first layer consists of soil, the second layer consists of rock fragments, and the third layer is limestone of the Kometan Formation. The first layer is weak and fissured and subjected to sinkholes buried with recent sediments. The third rock layer is harder to fracture than the first and second layers.

The dam failure is caused by many problems such as the basic design of the dam construction was not done scientifically, and uncontrolled water flows because the direction of water flow upstream is toward the west and exactly toward the southwestern part of the area, and the stress of water collected at the wall of the dam in this area that caused the failure of the dam wall in this region. The high features are concentrated in the north from west to east, while the low features are concentrated in the south, and some of the small and deep features are at the extreme of north and northeast. In the construction of the dam, compaction was not applied. The spillway was filled with rock fragments without concrete. The spillway should be constructed higher than the level of construction. The catchment area of the reservoir is small. At the beginning parts of most traverses, the presence of a sinkhole appeared, which is related to the filling of the layers with water during the winter rainy season, then the water penetrated deeply, which led to the layer collapse and forming this

sinkhole. This sinkhole in the western part can be considered the main cause of collapsing the dam after subjecting water pressure exerted on the dam.

References

Abdelwahed, B., 2019. A review on building progressive collapse, survey and discussion, Case Studies in Construction Materials, Elsevier, Volume 11, DOI:/10.1016/j.cscm.2019.e00264.

Abdulrahman, D. Z., 2014. Case study of the Chaq-Chaq dam failure: Parameter estimation and evaluation of dam breach prediction models. Journal of Engineering Research and Applications, Vol. 4, Issue 5, pp. 109-116.

Adamo, N., Al-Ansari, N., Sissakian, V., Laue, J., and Knutsson, S., 2020. Dam Safety and Earthquakes. Journal of Earth Sciences and Geotechnical Engineering, Vol. 10, No. 6, pp. 79-132.

Alavi, M., 2004. Regional stratigraphy of the Zagros Fold-Thrust Belt of Iran and its pro-foreland evolution. American Journal of Science, 304, pp. 1-20.

Alavi, M., 2007. Structures of the Zagros fold-thrust belt in Iran. American Journal of Science, 307(9), pp.1064-1095, DOI:10.2475/09.2007.02.

Al-Hakari, S.H.S., 2011. Geometric Analysis and Structural Evolution of NW Sulaimani Area, Iraq. The unpublished Ph.D. Thesis University of Sulaimani.

Al-Khafaf, A.O.S., 2005. Stratigraphy of Kometan Formation, Upper Cretaceous in Dokan-Endezah area, Northeastern Iraq. Unpublished M.Sc. Thesis, University of Mosul, 79p.

Al-Qayim, B., 1993. Petrofacies Analysis and Tectonic Evolution of a Zagroside Flysch Suites from Northeastern Iraq. In Kumon and Ku (Eds.), Petrology of Sandstones in Relation to Tectonics, V.S.P., Netherlands, pp. 33-42.

Al-Qayim, B., Ibrahim, A.O., and Koyi, H., 2012. Tectono Stratigraphic overview of the Zagros Suture Zone, Kurdistan Region, Northeast Iraq. GeoArabia, 2012, V17, No.4, pp. 109-156.

Andrea, D.V. Fisher, R.L. and Fagelaon, D. E., 1965. Prediction of Compressive Strength from other Rock properties, U.S.B.M., R.I.6702, 23 P.

Baban E.N., (2001). Geophysical study of selected regional lines in the Western Desert of Iraq, Ph.D. thesis (unpublished), University of Baghdad, Iraq.

Brosten, T. R., Llopis, J. L., and Kelley, J. R., 2005. Using geophysics to assess the condition of small embankment dams. USACE Engineering Research and Development Center, ERDC/GSL TR-05-17.

Buday, T., 1980. Regional Geology of Iraq: Vol. 1, Stratigraphy, I.I. Kassab and S.Z. Jassim (Eds) D. G. Geo Survey. Min. Invest. Publication. 445 P.

Buday, T., and Jassim, S.Z., 1987. The regional geology of Iraq (Tectonism, Magmatism and Metamorphism). Vol.2, Edited by Kassab, I.I. and Abbas, M. J., Geol. Surv. Min. Inves Baghdad, Iraq, 352 P.

Desper, D.B., Link, C.A., and Nelson, P.N., 2015. Accurate water-table depth estimation sing seismic refraction in areas of rapidly varying subsurface conditions: Near Surface Geophysics, v. 13, pp. 455-465.

Dhamiri, NM, and Zouaghi, T., 2020. Near-surface geophysical surveys for bedrock investigation and modeling for grain silos site, Yanbu City, Western Saudi Arabia. Modeling Earth Systems and Environment, 6 (1), 51-61.

Dutta, N. P., 1984. Seismic refraction method to study the foundation rock of dam. Geophysical Prospecting, 32, pp. 1103 – 1110. Earth view, 2022. Earth view-map 3D, https://wolfsys.net/earth-view-map-3d.

FAO, 2001. Geophysical report of proposed Chaqchaq dam, personal communication.

Google Earth Pro, 2022. https://earth.google.com/web/@35.60519814,45.37444929,848.97739863a,16777.06932493d,35y,-0h,0t,0r

Jassim, S. Z., and Goff, J. C., 2006. Geology of Iraq, 1st. Edited by Lea Novotna. Dolin, Hlavni 2732, Prague and Moravian Museum, Zelny trh 6, Brno, Czech Republic, 341 P.

Jemes, L.D., Melanie, A.S., Bengston, L., 1986. Catastrophic Damage from Dam Break Floods. Utah Water Research Laboratory, Utah State University DigitalCommons@USU.

Karim K. H., Ismael, K. M., Ameen., B. M., 2008. Lithostratigraphic study of the contact between Kometan and Shiranish formations (Cretaceous), in Sulaimaniyah governorate, Kurdistan region, NE Iraq. Iraqi Bulletin of Geology and Mining, Vol.4, No.2, pp. 15-27.

Khaleel, A., 2013. Urban Geomorphology of Sulaimani City, Using Remote Sensing and GIS Techniques, Kurdistan Region, Iraq. Ph.D. thesis (unpublished), pp. 1-253. Khalil, M.H. and Hanafy, S.M., 2008. Engineering application of seismic refraction method; a field example at Wadi Wardan. NE, Sinai, Egypt, Journal of Applied Geophysics, no.65.

Manual of Geometrics Inc., 2021. Geometrics, Resources. Made in USA Company. https://geometrics.com/resources/

Mirassi, S., and Rahnema, H., 2020. Deep cavity detection using propagation of seismic waves in homogenous half-space and layered soil media. Asian Journal of Civil Engineering 21:1431–1441, DOI:10.1007/s42107-020-00288-2

Palmer, D., 1986. Refraction seismics: In: Helbig, K., and Treitel, S., (eds): Handbook of Geophysical Exploration. Section 1. Seismic Exploration, Vol. 13, Geophysical press, London-Amsterdam, pp. 1-265.

Petaccia, G., Lai, C. G., Milazzo, C., and Natale, L., 2016. The collapse of the Sella Zerbino gravity dam. Engineering geology, 211, pp. 39-49. https://doi.org/10.1016/j.enggeo.2016.06.024

Potter, C. and Fottinek, D., 1997. Elastic Parameters by Deriving S- Wave Velocity Logs: CREWS Research Report, 9: pp. 1-10.

Reynolds, J. M., 2011. An introduction to applied and environmental geophysics. John Wiley and Sons.

Sarris, A., Kalayci, T., Moffat, I., Manataki, M., 2018. An Introduction to Geophysical and Geochemical Methods in Digital Geoarchaeology. In: Siart, C., Forbriger, M., Bubenzer, O. (eds) Digital Geoarchaeology. Natural Science in Archaeology. Springer, Cham., DOI:10.1007/978-3-319-25316-914

Sharafeldin, M., Sharafeldin, 2008. Seismic Refraction Survey to Characterize Bedrock of Dam and Reservoir Site, Wadi Asala, Jeddah Area, Saudi Arabia. Journal of Applied Geophysics, Vol. 7, No. 1, pp. 265-286.

Tezcan, S.S., Keceli, A. and Ozdemir, Z., 2006. Allowable Bearing Capacity of Shallow Foundations Based on Shear Wave Velocity. Geotechnical Geology Engineering, 24, 203–218, DOI:/10.1007/s10706-004-1748-4

UFC (Unified Facilities Criteria), 2008. "Structures to Resist the Effects of Accidental Explosions", UFC 3-340-02, Department of Defense, US Army Corps of Engineers, Naval Facilities Engineering Command, Air Force Civil Engineer Support Agency, United States of America.

Uyank, O., 2011. The porosity of saturated shallow sediments from seismic compressional and shear wave velocities. Journal of Geophysics, 73, pp. 16-24.

Xia, J., Miller, R.D., and Park, C.B., (1999). "Estimation of near surface shear-wave velocity by inversion of Rayleigh waves". Geophysics, 64, 691-700.

Zebari, M., Grützner, C., Navabpour, P., and Ustaszewski, K., 2019. Relative timing of uplift along the Zagros Mountain Front Flexure (Kurdistan Region of Iraq): Constrained by geomorphic indices and landscape evolution modeling. Solid Earth, 10, pp. 663–682, DOI:10.5194/se-10-663-2019